

1 **Evaluation of atmospheric model parameterization
2 schemes with river network routing and streamflow
3 observations: A case study of the Yarlung Zangbo
4 River on the Tibetan Plateau**

5 **Heng Yang¹, Shuanglong Chen², Qingyun Bian³, and Hui Zheng³**

6 ¹Science and Technology Research Institute, China Three Gorges Corporation, Beijing 100038, China

7 ²Baihetan Hydropower Plant, China Three Gorges Corporation, Sichuan 615421, China

8 ³Institute of Atmospheric Physics, Chinese Academy of Sciences, Beijing 100029, China

9 **Key Points:**

- 10 • A river network routing-based method is developed to evaluate atmospheric mod-
11 els using streamflow observations
- 12 • High skill in streamflow correlation coefficient corresponds to superiority in mod-
13 eling the spatial distribution of precipitation
- 14 • Shortwave radiation parameterization has a minimal impact on precipitation es-
15 timation but a notable impact on runoff and streamflow

Abstract

Evaluating kilometer-scale atmospheric models in data-sparse regions with complex topography, such as the Tibetan Plateau, presents inherent challenges due to the scarcity of in-situ observations and uncertainties in remote-sensing data. Hydrological evaluation, which utilize hydrological models to connect atmospheric model-simulated precipitation with streamflow observations, are hindered by model structural and parameter uncertainties, particularly significant in high-altitude mountainous basins. This study introduces a river network routing-based method that calculates streamflow directly from atmospheric model-simulated runoff, making fewer assumptions and thus being more adaptable to high-altitude mountainous basins. We applied this method to assess 3-kilometer Weather Research and Forecasting model simulations over the Yarlung Zangbo River on the Tibetan Plateau, each configured with distinct parameterizations for microphysics, planetary boundary layer, and shortwave radiation. The streamflow evaluation was compared with an evaluation of precipitation against satellite data. Results indicate that the streamflow evaluation complements the precipitation evaluation effectively. The WRF simulation that excelled in reproducing precipitation amounts and temporal variations also demonstrated the best performance in estimating streamflow's mean and variability. Furthermore, the river routing-based evaluation of streamflow offers additional insights beyond the precipitation evaluation. While the shortwave radiation parameterization had negligible impacts on precipitation amount, its influence on streamflow was significant. The experiment utilizing the Dudhia radiation scheme achieved the best temporal correlation with streamflow observations, corresponding to an accurate representation of spatial precipitation patterns as evaluated against satellite data. The findings underscore the value of the river network routing-based method in evaluating atmospheric models, especially in data-sparse and topographically complex regions.

1 Introduction

In recent years, the resolution of atmospheric models has gradually increased, reaching grid spacings as fine as 5 kilometers or less. These high-resolution, kilometer-scale models have largely overcome the need for deep convection parameterizations, thereby eliminating a significant source of uncertainty that was previously inherent in coarser-resolution models (Prein et al., 2015; Mooney et al., 2017). Moreover, kilometer-scale atmospheric simulations are capable of capturing the intricate effects of fine-scale topog-

48 raphy on atmospheric circulation patterns, particularly in mountainous regions (C. Lin
49 et al., 2018; Zhou et al., 2021; Yuan et al., 2023; Sugimoto et al., 2021; Ma et al., 2023;
50 Li et al., 2022). The explicit representation of deep convection and meticulous attention
51 to topographic detail have substantially enhanced the accuracy of the estimation of hy-
52 drological gradient along terrain slopes (Jiang, Yang, Yang, et al., 2022; Sugimoto et al.,
53 2021; Ma et al., 2023).

54 In mountainous regions characterized by strong hydrological gradients, such as the
55 Tibetan Plateau, kilometer-scale atmospheric models are particularly useful (Prein et
56 al., 2023). Mountainous regions experience pronounced hydrological gradients (Immerzeel
57 et al., 2014) that are undergoing substantial changes due to global climate change (Yao
58 et al., 2019; Cui et al., 2023; T. Wang et al., 2021; Kraaijenbrink et al., 2021). The scarcity
59 of in-situ observations and the inherent uncertainties in remote-sensing products impede
60 the accurate monitoring of these hydrological changes (Miao et al., 2024). Evidence sug-
61 gests that kilometer-scale atmospheric models can achieve an accuracy that surpasses
62 that of in-situ observations (Lundquist et al., 2019) and even satellite-based products
63 (Jiang, Yang, Li, et al., 2022). Moreover, these models are indispensable for projecting
64 future water resources in the context of a changing climate (Prein et al., 2023).

65 In mountainous regions, accurately evaluating kilometer-scale atmospheric mod-
66 els presents a formidable challenge. Meteorological observations are frequently confined
67 to select locations within river valleys, leaving vast areas unmonitored. Remote locales,
68 such as mountain peaks and barren lands, are known to contribute significantly to wa-
69 ter sources but are often overlooked in observational data (Miao et al., 2024). The com-
70 plex topography and frozen ground in these areas can significantly distort remote-sensing
71 products, including satellite-based precipitation estimates (Behrang et al., 2014). Con-
72 sequently, the scarcity of in-situ meteorological observations and the associated uncer-
73 tainties in remote-sensing data render the assessment of kilometer-scale atmospheric mod-
74 els less conclusive.

75 Hydrological evaluation serves as an enlightening approach for assessing the per-
76 formance of atmospheric models in mountainous regions. This technique entails utiliz-
77 ing the precipitation data simulated by an atmospheric model to drive a hydrological model.
78 Subsequently, the resulting streamflow is compared against observed streamflow (Krier
79 et al., 2012; Henn et al., 2015, 2016; Pang et al., 2020). However, the application of a

hydrological model requires a significant array of assumptions concerning model structure and parameterization (Kirchner, 2009; Henn et al., 2016). These assumptions can be rigorously tested in data-rich regions (Clark et al., 2011; Zheng et al., 2020) but are largely unconstrained in data-sparse regions, such as the Tibetan Plateau. There exists the potential for such uncertainties to be so pronounced that distinguishing the simulated precipitation from the observed streamflow becomes an ill-posed problem (Renard et al., 2010). Different combinations of precipitation and hydrological models may yield similar streamflows that align with observations. Due to the significant uncertainty inherent in hydrological models and limited fidelity constraints in such case, the inclusion of low-fidelity hydrological models in the evaluation process, particularly when they contribute to the best streamflow estimates, may inadvertently lead to an erroneous assessment of the atmospheric model's performance. This concern is particularly pertinent to high-altitude mountainous basins, such as the Yarlung Zangbo River basin, where considerable model structural and parameter uncertainty has been found in our previous study (Lei et al., 2024).

Hydrological models primarily capture two fundamental processes in mountainous basins: runoff generation and river routing. Despite the intricate nature of runoff-generation processes in mountainous regions (van Tiel et al., 2024), the dynamics of water flow are often less complex than those observed over flat terrains (Getirana & Paiva, 2013; Moussa & Bocquillon, 1996). Characterized by steep slopes, mountain rivers enable water flow to be primarily represented using the kinematic wave approximation of the Saint-Venant equations (Moussa & Bocquillon, 1996). This representation indicates that the flow is predominantly influenced by the interplay between friction and channel slope (Getirana & Paiva, 2013; Moussa & Bocquillon, 1996). Given that river channel slopes can be extracted globally from high-resolution digital elevation models (Yamazaki et al., 2017, 2019), the routing of water flow in mountainous basins is heavily reliant on assumptions about channel friction. While the friction assumption makes a relatively minor component within the previously discussed hydrological models, characterizing uncertainties in channel friction is often more straightforward than addressing the structural and parameter uncertainties inherent to hydrological models. The simplicity and robustness of the routing process in mountainous basins enhance its adaptability for evaluating atmospheric models in these regions.

In the light of the aforementioned findings, we propose an alternative approach to evaluating atmospheric models that leverages river network routing. This approach involves directly routing the runoff simulated by atmospheric models through the river network to generate streamflow estimates at gauge locations. The method streamlines the evaluation process by circumventing the complexities of runoff generation processes, which are now integrated within the atmospheric model. The atmospheric models are capable of more effectively constraining the runoff generation processes than hydrological models, due to their ability to account for surface energy and water balance dynamics as well as land-atmosphere interactions (Wagner et al., 2016; Senatore et al., 2015). We contend that this river network routing-based method is particularly well-suited for data-sparse and topographically complex regions such as the Tibetan Plateau, providing a more targeted and effective means of model evaluation.

In this study, we have implemented our proposed method to evaluate the simulations produced by the Weather Research and Forecasting (WRF) model (Powers et al., 2017), specifically applied to the Yarlung Zangbo River, the most significant river on the Tibetan Plateau. The structure of this paper is as follows: Section 2 delineates the methodologies and datasets utilized within our research. Section 3 details the outcomes and ensuing discussions. Finally, Section 4 synthesizes the findings and concludes the study.

2 Methods and Data

2.1 Experimental Design

Figure 1 illustrates the workflow of this study. We conducted a series of five 3-kilometer WRF experiments from May 1 to October 1, 2013, encompassing the wet season of the year. The experiments were configured with various parameterization schemes for cloud physics, planetary boundary layer, and shortwave radiation. The objective was to identify the optimal parameterization scheme using the streamflow observations from four river gauges along the Yarlung Zangbo River, namely Lazi, Nugesha, Yangcun, and Nuxia, arranged from upstream to downstream.

The WRF experiments were initialized and driven by data from the European Centre for Medium-Range Weather Forecasts Reanalysis version 5 (ERA5) (Hersbach et al., 2020). Following this, the runoff simulated by WRF was spatially re-mapped to account for lateral inflow into the river network. The river flow within this network was then routed

143 using the Muskingum method, a well-established approach for routing mountainous river
144 flows. We tested a range of routing parameter values, calibrating them against stream-
145 flow observations to identify the optimal value for each segment of the river network sit-
146 uated between two river gauges. Subsequently, the WRF experiments were intercompared
147 and assessed based on the accuracy of streamflow estimation using these optimal rout-
148 ing parameters.

149 **2.2 Observational Data**

150 We utilized streamflow data provided by the China Three Gorges Corporation, col-
151 lected at four river gauges along the Yarlung Zangbo River: Lazi, Nugesha, Yangcun,
152 and Nuxia. Instantaneous streamflow observations were recorded at 00:00 UTC daily from
153 June 20 to October 1, 2013. These data were instrumental in optimizing the routing pa-
154 rameter and evaluating the estimated streamflow for the WRF experiments.

155 To intercompare the river network routing-based evaluation of streamflow with the
156 widely adopted precipitation evaluations based on remote sensing products, we also em-
157 ployed the Global Precipitation Measurement (GPM) Multi-satellitE Retrievals for GPM
158 (IMERG) product (Huffman et al., 2019). The IMERG product offers data at a spatial
159 resolution of 0.1° by 0.1° and a temporal resolution of 30 minutes. We applied bilinear
160 interpolation to downscale the GPM data to align with the 3-kilometer resolution of the
161 WRF grid.

162 **2.3 Study Area and River Network**

163 Figure 2 displays the modeling domain of the WRF model, which spans 380 by 660
164 grid cells, each measuring 3 by 3 kilometers. The domain covers the entire Yarlung Zangbo
165 River basin and extends to include a buffer zone that surrounds the river basin. This buffer
166 zone, which is over 200 kilometers wide, is strategically designed to accommodate the
167 development of small-scale weather systems before they interact with the river basin (Denis
168 et al., 2002). This design helps to reduce the adverse effects stemming from inaccurate
169 or low-resolution boundary conditions.

170 The routing was performed on the river network as illustrated in Figure 2. The river
171 network was delineated from the Multi-Error Removed Improved-Terrain Hydrography
172 (MERIT-Hydro) dataset (Yamazaki et al., 2017, 2019), which offers flow directions and

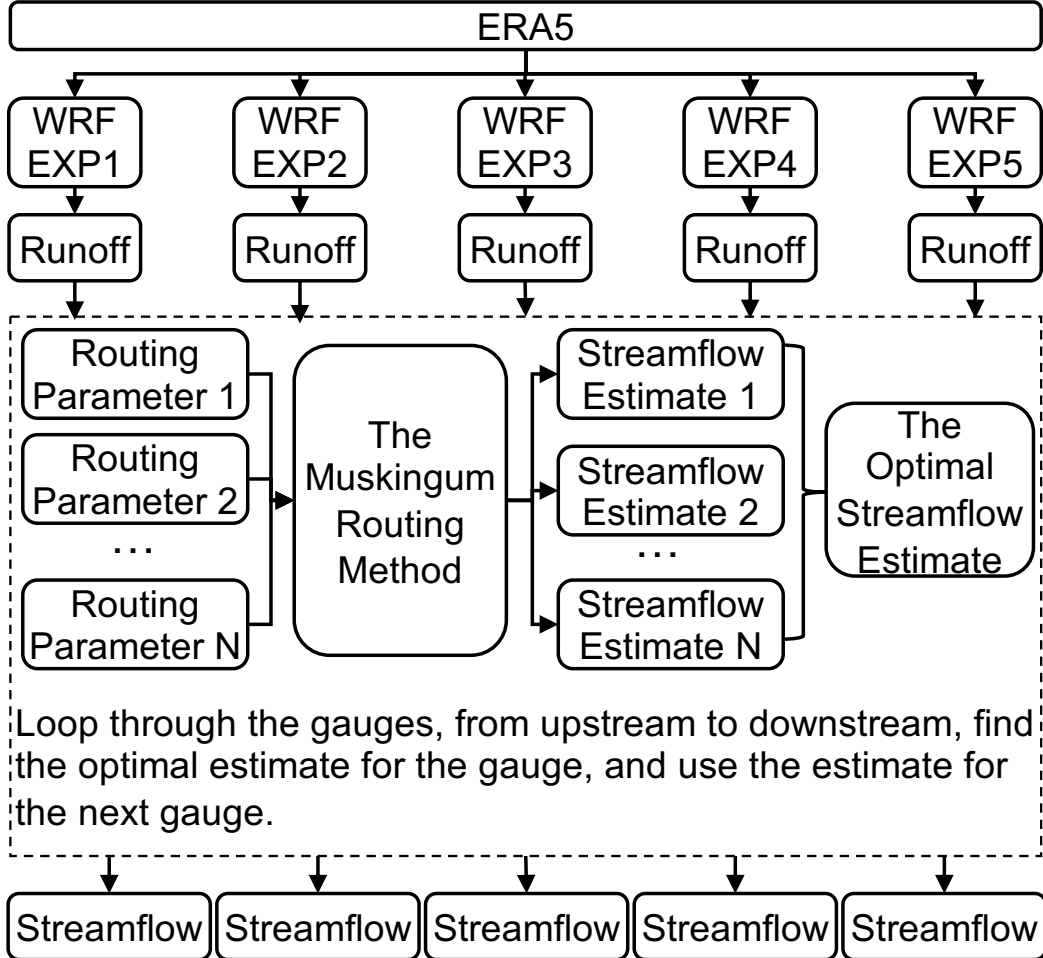


Figure 1. Schematic diagram of the workflow of this study.

173 accumulative upstream area data at a spatial resolution of 3 by 3 arcseconds. The de-
 174 delineation process unfolds in three sequential steps: Initially, the accumulative upstream
 175 area is employed to identify river centerlines, with a grid cell being classified as such if
 176 its accumulative upstream area surpasses 10 km^2 . Subsequently, these centerlines are seg-
 177 mented into river reaches from upstream to downstream, defining a reach by an increase
 178 in the ccumulative upstream area of at least 20 km^2 along its path. Finally, the flow di-
 179 rection data is utilized to determine the catchment area of each reach, encompassing all
 180 grid cells that contribute flow directly to the reach. The thresholds for defining river cen-
 181 terlines and segmenting river reaches align with those used in previous large-domain river
 182 routing studies (P. Lin et al., 2021, 2019). This delineation process results in a fully con-
 183 nected river network consisting of 5,800 reaches.

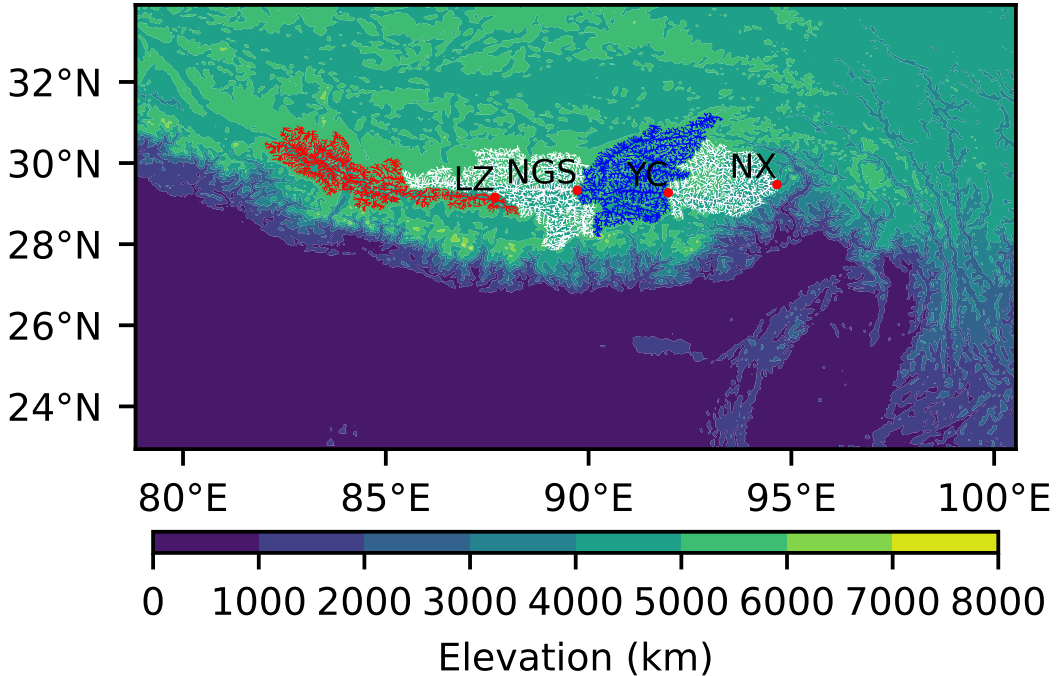


Figure 2. Modeling Domain and Delineated River Network of the Yarlung Zangbo River. The colormap provides a representation of the terrain elevation, showcasing the basin's topographical characteristics. Red dots indicate the locations of the four river gauges along the river's course, labeled as follows: LZ for Lazi, NGS for Nugesha, YC for Yangcun, and NX for Nuxia from upstream to downstream. The differently colored lines correspond to the river reaches that lie between consecutive gauges, offering a visual guide to their spatial distribution across the basin.

2.4 WRF Parameterization Schemes

Table 1 lists the parameterization schemes chosen from WRF version 4.3.1 for the experiments. EXP1 serves as the baseline experiment, configured similarly to the High Asian Refined Analysis version 2 (X. Wang et al., 2021) with the exception of the radiation and land surface processes. Instead of the Rapid Radiative Transfer Model (RRTM) scheme (Mlawer et al., 1997), the RRTM for GCMs (RRTMG) (Iacono et al., 2008) was employed for shortwave and longwave radiation transfer. RRTMG is comparable to RRTM in terms of modeling radiative forcing but offers greater computational efficiency (Iacono et al., 2008). For the land surface processes, the Noah land surface model with multi-parameterization options (Noah-MP) (Niu et al., 2011; Z.-L. Yang et al., 2011) was selected in place of the Noah model used in HARR version 2. Noah-MP has been enhanced over the original Noah model, providing an improved representation of snow and runoff

processes (Niu et al., 2011). These enhancements have led to better performance in modeling runoff (Liang et al., 2019; Zheng et al., 2023), leading to the widespread adoption of Noah-MP in hydrological applications (Cosgrove et al., 2024; P. Lin, Hopper, et al., 2018).

Building on EXP1, EXP2 through EXP5 are designed to investigate the impacts of cloud microphysics, planetary boundary layer, and shortwave radiation, one parameterization at a time. These parameterizations have demonstrated their significance in previous studies (Lv et al., 2020; Prein et al., 2023). EXP2 and EXP3 vary from EXP1 in their cloud microphysics schemes. EXP1 employs the Thompson scheme (Thompson et al., 2008), whereas EXP2 utilizes the Purdue Lin scheme (Chen & Sun, 2002), and EXP3 incorporates the WRF Single-Moment 6-Class Microphysics (WSM6) scheme (Hong & Lim, 2006). EXP4 diverges from EXP1 in its planetary boundary layer scheme. Instead of the Mellor-Yamada-Janjić scheme (Janjić, 1994), EXP4 adopts the Yonsei University scheme (Hong et al., 2006). EXP5 differs from EXP1 in its radiation scheme, opting for the Dudhia scheme (Dudhia, 1989) for shortwave radiation transfer.

Table 1. WRF experiments and the used parameterization schemes.

Experiment	Cloud Microphysics	Planetary Boundary Layer	Shortwave Radiation
EXP1	Thompson	MYJ	RRTMG
EXP2	Purdue Lin	MYJ	RRTMG
EXP3	WSM6	MYJ	RRTMG
EXP4	Thompson	YSU	RRTMG
EXP5	Thompson	YSU	Dudhia

2.5 River Network Routing Method

The WRF-simulated runoff is re-mapped to represent lateral inflow into the rivers, following the remapping method detailed in (P. Lin, Yang, et al., 2018; S. Wang et al., 2019). For each river reach within the network, the WRF grid cells that intersect with the catchment area of the reach are first identified. The runoff volume from these grid cells is then calculated by multiplying the runoff depth by the area of intersection for

each cell. These individual values are subsequently summed to ascertain the total lateral flow volume entering the reach. Given the steep topography and extensive watershed area characteristic of the study region, terrain routing is intentionally omitted in this study to focus on the primary river flow dynamics and streamline the computational process.

We employ the Muskingum method to route water flow within the river network. This method is well-suited to characterize the flow's kinematic wave propagation that driven by the topographic gradient (Ponce et al., 1978). The formulation of the Muskingum method (Cunge, 1969; Fenton, 2019), when incorporating lateral inflows, can be expressed as follows:

$$Q_i^t = \frac{k - x}{1 - x + k} Q_{i-1}^t + \frac{1 - x - k}{1 - x + k} Q_i^{t-1} + \frac{x + k}{1 - x + k} Q_{i-1}^{t-1} + \frac{2k}{1 - x + k} Q_l^t, \quad (1)$$

$$k = \frac{c\Delta t}{2\Delta l}, \quad (2)$$

where Q_i^t ($\text{m}^3 \text{s}^{-1}$) is the streamflow of a reach at current time step, Q_{i-1}^t ($\text{m}^3 \text{s}^{-1}$) is the streamflow at the upstream position of the reach at current time step, Q_i^{t-1} ($\text{m}^3 \text{s}^{-1}$) is the streamflow of the reach at previous time step, Q_{i-1}^{t-1} ($\text{m}^3 \text{s}^{-1}$) is the streamflow at the upstream position at the previous time step, Q_l^t ($\text{m}^3 \text{s}^{-1}$) is the lateral inflow entering the reach at current time step. Δt is the time step (s), and Δl is the reach length (m). x is the weighting factor (unitless), and c is the wave celerity (m s^{-1}).

The application of the Muskingum method to the reaches of a fully connected river network must be executed in the correct order. When routing the streamflow of a reach, the discharge at the reach's upstream position must be available. We sorted all the river reaches with the network according to the stream order as introduced in (X. Yang et al., 2024). This sorting ensures that upstream reaches are always prioritized over their downstream reaches. Subsequently, we apply the Muskingum method to each reach in the established sequence. This sequence guarantees that routing on upstream reaches is conducted first, followed by routing on downstream reaches.

The Muskingum method includes two adjustable routing parameters: the weighting factor (x ; unitless) and wave celerity (c ; m s^{-1}). The weighting factor x is used to regulate the proportional contributions of the right-hand-side terms in Equation 1. Studies have shown that the simulated streamflow is relatively insensitive to variations in the weighting factor (Koussis, 1978). Values ranging from 0.1 to 0.3 are typically effective

246 for most streams. Guided by the experiments reported by David et al. (2011), we have
 247 chosen a parameter value of 0.3 for this study.”

248 The wave celerity c represents the speed at which the flow wave propagates down-
 249 stream and is influenced by the physical characteristics of the river channel, including
 250 channel slope, roughness, and width. Given that direct observations of c are unavailable
 251 for the Yarlung Zangbo River basin, we conducted a series of simulations with varying
 252 wave celerity values. We selected the value that best aligns with the streamflow obser-
 253 vations, which is considered representative of the river channel’s physical characteristics.
 254 The optimal wave celerity value c is determined for each streamflow gauge in an upstream-
 255 to-downstream sequence. Once a wave celerity value is chosen for a gauge, it is applied
 256 to all downstream gauges. This process is repeated sequentially until wave celerity val-
 257 ues are selected for all streamflow gauges.

258 2.6 Evaluation Metrics

259 We utilized the Pearson correlation coefficient to identify the optimal wave celer-
 260 ity value. The Pearson correlation coefficient (r) is defined as follows:

$$r = \frac{\sum_{i=1}^n (x_i - \bar{x})(y_i - \bar{y})}{\sqrt{\sum_{i=1}^n (x_i - \bar{x})^2 \sum_{i=1}^n (y_i - \bar{y})^2}}, \quad (3)$$

261 where x_i and y_i are the simulated and observed streamflow at time step i , respectively.
 262 \bar{x} and \bar{y} are the mean of the simulated and observed streamflow, respectively. The Pear-
 263 son correlation coefficient ranges from -1 to 1 , with a value of 1 indicating a perfect pos-
 264 itive linear relationship between the simulated and observed streamflow. This coefficient
 265 is insensitive to biases in the streamflow estimates, making us to focus on daily scale stream-
 266 flow variations in this study.

267 We used the Kling–Gupta efficiency (KGE) (Gupta et al., 2009) to intercompare
 268 the WRF parameterization schemes. KGE systematically summarizes how a hydrolog-
 269 ical simulation matches observations in correlation, standard deviation, and bias. The
 270 KGE is defined as follows:

$$\text{KGE} = 1 - \sqrt{(r - 1)^2 + (\alpha - 1)^2 + (\beta - 1)^2}, \quad (4)$$

$$\alpha = \frac{\sigma}{\sigma_o}, \quad (5)$$

$$\beta = \frac{\mu_s}{\mu_o}, \quad (6)$$

271 where r is the Pearson correlation coefficient between the simulation and observation,
 272 σ is the standard deviation of the simulation, and μ is the mean. The subscripts s and
 273 o denote the simulated and observed values, respectively. The KGE ranges from $-\infty$ to
 274 1. A KGE value of 1 indicates a perfect match between the simulated and observed stream-
 275 flow.

276 3 Results and Discussion

277 In this section, we first intercompares the WRF-simulated precipitation and runoff.
 278 Subsequently, we assess the streamflow estimates by comparing them against observed
 279 streamflow data.

280 3.1 Intercomparison of the WRF-simulated precipitation and runoff

281 Figure 3 displays the spatial distribution of simulated precipitation from the five
 282 WRF experiments. The patterns from EXP1 through EXP3 exhibit close agreement, with
 283 two primary precipitation centers evident downstream of Yangcun and between Lazi and
 284 Nugesha. Notably, the precipitation intensity between Lazi and Nugesha is slightly higher.
 285 In comparison to the baseline EXP1, the distribution in EXP5 appears more dispersed,
 286 featuring a significant precipitation center downstream of Yangcun, as shown in Figure 3e.
 287 EXP4 closely mirrors the spatial pattern of EXP5, with a spatial correlation coefficient
 288 of 0.93 achieved between them. However, EXP4 (Figure 3d)exhibits the weakest precip-
 289 itation intensity among the experiments. The experiments show greater consensus in the
 290 downstream areas of the Yarlung Zangbo River than in the headwater regions, as indi-
 291 cated in Figure 3f. When juxtaposed with the GPM data, there is a tendency for all five
 292 experiments to overestimate the precipitation rate.

293 Figure 4 presents the time series of accumulated precipitation, averaged across the
 294 catchments of the four river gauges. Consistent with the spatial distribution depicted
 295 in Figure 3, all five WRF experiments exceed the GPM precipitation rate across all four
 296 catchments. The variation among the experiments is considerable. The disparity between
 297 EXP4 and EXP1 underscores the significant influence of the planetary boundary layer
 298 on precipitation. This finding aligns with the results reported by Prein et al. (2023), sug-
 299 gesting that the impact of planetary boundary layer parameterization can be more pro-
 300 nounced than that of cloud physics, as evidenced by the differences between EXP1 and

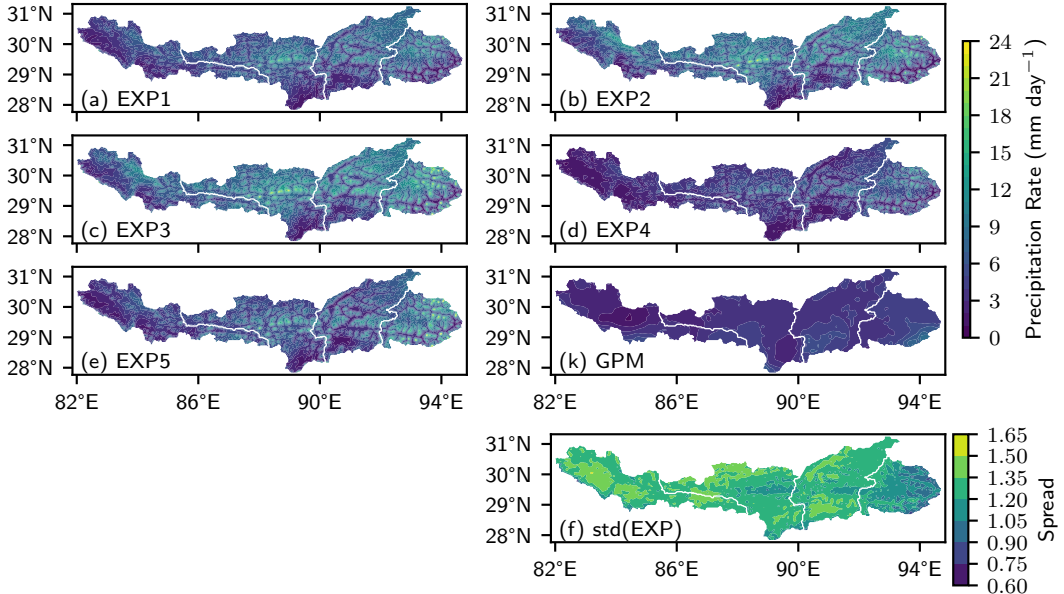


Figure 3. Spatial distribution of the precipitation rate averaged from June 20 to October 1, 2013. (a)–(e) The five WRF experiments described in Table 1. (k) The GPM precipitation. (f) the ensemble spread of the five experiments measured in standard deviation. The white lines denotes the division of the river network between two river gauges.

301 EXP2, and between EXP1 and EXP3. The difference between EXP5 and EXP1 is neg-
 302 ligible across all four catchments, indicating that the parameterization of shortwave ra-
 303 diation has a minimal impact on the simulation of precipitation.

304 Table 2 presents the skill of the WRF experiments as measured against GPM data.
 305 The cloud physics parameterization significantly influences the timing of precipitation,
 306 leading to substantial changes in the correlation coefficient (r) for EXP2 and EXP3 rel-
 307 ative to EXP1. A comparison between EXP4 and EXP1 indicates that the planetary bound-
 308 ary layer parameterization has a minimal impact on precipitation timing. However, there
 309 are notable differences in the amount of precipitation (β) and its variability (α), suggest-
 310 ing the importance of the planetary boundary layer in moisture transport for precipi-
 311 tation (Y. Wang et al., 2020). Although the shortwave radiation parameterization has
 312 a minimal impact on the amount of precipitation (β), it significantly affects the mag-
 313 nitude of precipitation variability (α), particularly in the middle reaches of the Yarlung
 314 Zangbo River between Lazi and Yangcun. The reason for this impact is not yet clear.
 315 However, offline studies in this area (Lei et al., 2024) have found that shortwave radi-

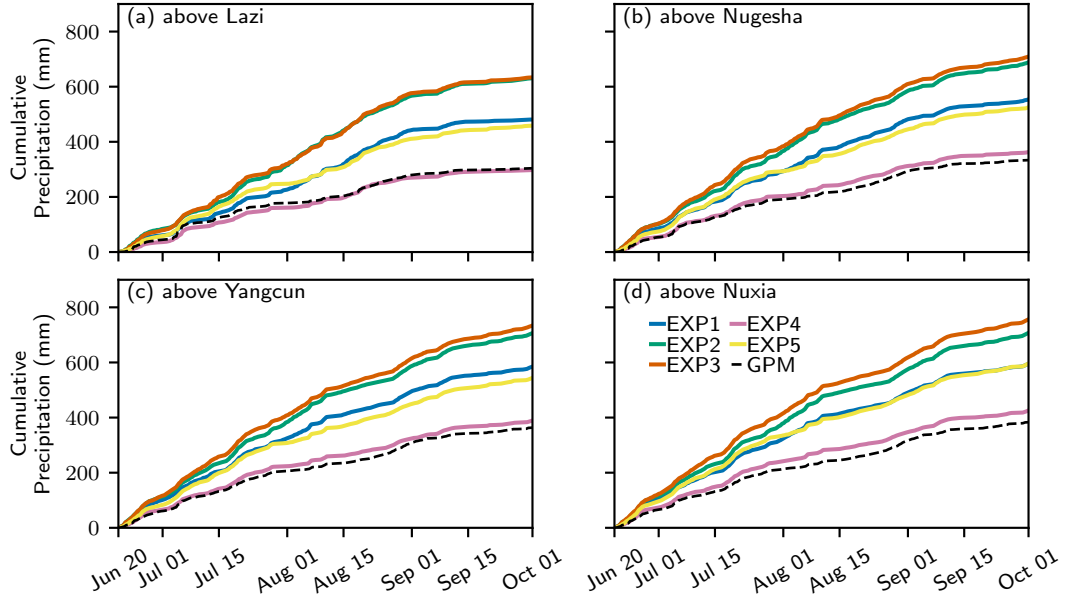


Figure 4. Time series in the accmulated precipitation averaged over the areas above (a) Lazi, (b) Nugesha, (c) Yangcun, and (d) Nuxia.

ation significantly affects the land surface energy and water budgets. We hypothesize that the changes in precipitation may be a consequence of local land-atmosphere interactions originated from the changes in land surface energy budgets.

Figure 5 presents the time series of accumulated runoff, averaged across the catchments of the four river gauges. The accumulated runoff for the specified period correlates well with the precipitation data. The accumulated runoff for the specified period exhibits a strong correlation with the precipitation data. Among the five experiments, EXP2 and EXP3 produce the highest runoff estimates, with their performances being closely aligned. In contrast, EXP4 records the lowest runoff, and its deviation from EXP1 is more significant than the difference observed between EXP1 and EXP2. The disparity in runoff between EXP5 and EXP1 is considerably larger than the difference in their respective precipitation estimates, especially in the upper reaches of the Yarlung Zangbo River, as shown in Figures 5b and 5c. This pronounced difference in runoff is anticipated to result in variations in the streamflow estimates, which will be further analyzed in the subsequent sections.

Table 2. Kling–Gupta efficiency of the hourly precipitation rate averaged within the catchment of the river gauges. Italic fonts indicate the experiment that best matches GPM.

	Metric	LZ	NGS	YC	NX
EXP1	KGE	0.32	0.25	0.30	0.36
	α	1.06	1.22	1.22	1.22
	β	1.58	1.66	1.60	1.55
	r	0.65	0.72	0.73	0.75
EXP2	KGE	-0.23	-0.22	-0.10	0.00
	α	1.27	1.39	1.37	1.37
	β	2.07	2.06	1.94	1.85
	r	0.46	0.53	0.56	0.60
EXP3	KGE	-0.19	-0.23	-0.12	-0.07
	α	1.22	1.36	1.34	1.34
	β	2.08	2.12	2.01	1.97
	r	0.58	0.65	0.67	0.69
EXP4	KGE	0.61	0.72	0.73	0.75
	α	0.75	0.94	0.94	0.97
	β	0.98	1.09	1.07	1.11
	r	0.70	0.74	0.75	0.77
EXP5	KGE	0.39	0.35	0.42	0.38
	α	0.94	1.11	1.09	1.14
	β	1.51	1.57	1.49	1.55
	r	0.67	0.72	0.71	0.74

3.2 Evaluation against streamflow observations

Figure 6 demonstrates the changes in the correlation coefficient of streamflow with celerity across the four river gauges. Table 3 lists the optimal celerity values for each gauge

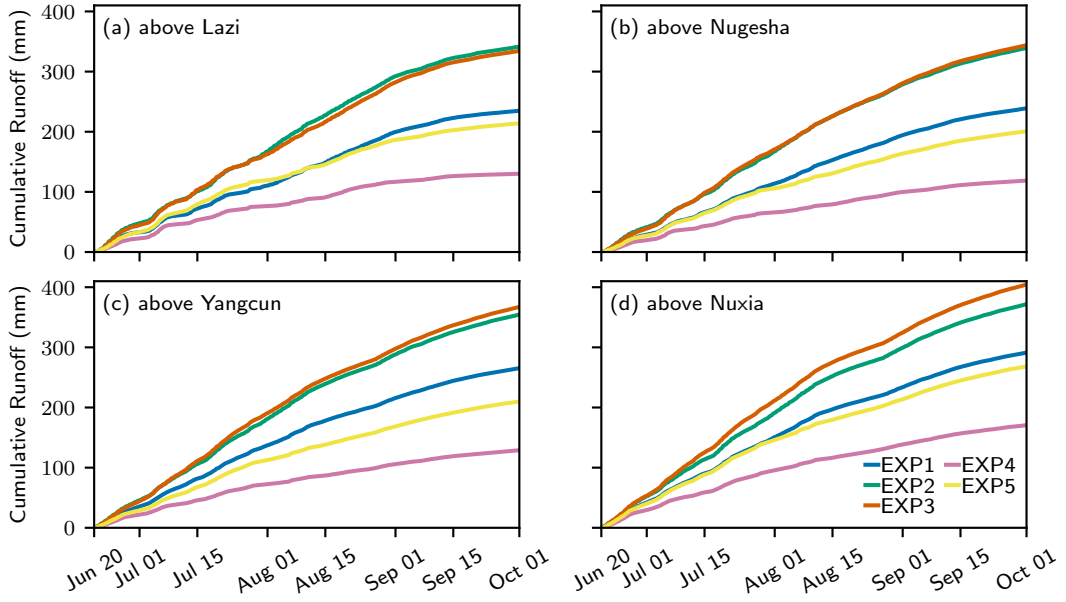


Figure 5. Time series in the accumulated runoff averaged over the areas above (a) Lazi, (b) Nugesha, (c) Yangcun, and (d) Nuxia.

corresponding to the WRF experiments. The variation of the correlation coefficient with celerity and the optimal celerity values exhibit consistency across all five experiments. This consistency supports the notion that celerity is predominantly determined by the river channel characteristics in mountainous basins. Specifically, the optimal celerity in the upstream segment of the main channel is generally slower compared to that in the downstream segment. As shown in Figure 2, the downstream area, located at the edge of the Tibetan Plateau, is characterized by a broader river channel and a more pronounced slope, which likely contributes to the observed celerity differences.

Table 3. The optimal flow wave celerity.

	LZ	NGS	YC	NX
EXP1	0.4	1.4	1.5	2.4
EXP2	0.4	1.2	1.5	3.0
EXP3	0.4	1.6	1.5	2.2
EXP4	0.4	1.1	1.2	1.5
EXP5	0.4	1.3	1.2	1.9

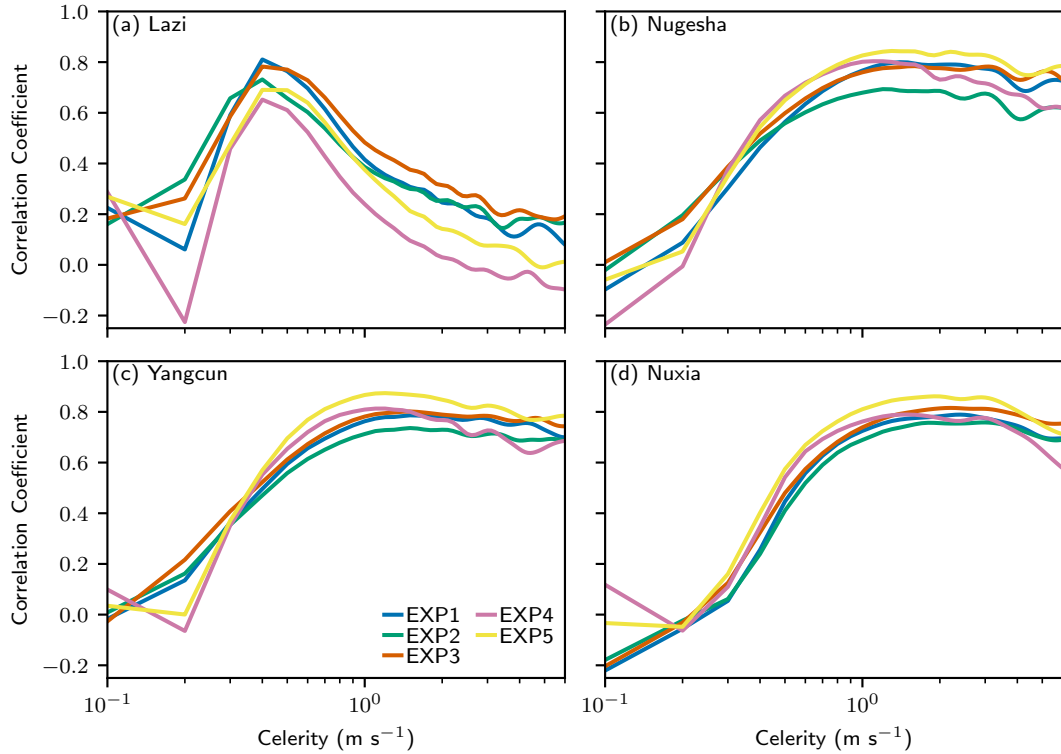


Figure 6. Sensitivity of streamflow modeling skill to wave celerity at the four river gauges.

(a) Lazi, (b) Nugesha, (c) Yangcun, and (d) Nuxia.

342 Figure 7 displays the time series of streamflow estimates for the five WRF expe-
 343 riments at the four river gauges. Table 4 provides a detailed assessment of the skill of these
 344 estimations. Consistent with the observations in precipitation and runoff, there are no-
 345 table differences in streamflow estimates among the experiments. While EXP4 demon-
 346 strated the best performance across all metrics in the evaluation of precipitation against
 347 GPM, its advantage in streamflow is primarily observed in terms of bias and in the Kling-
 348 Gupta Efficiency (KGE) at the upper to middle reaches. The KGE value for EXP4 in-
 349 creases progressively from upstream to downstream, with a value of -1.78 at the Lazi gauge
 350 and improving to 0.69 at the Yangcun gauge. At the most downstream gauge, Nuxia,
 351 EXP5 outperforms EXP4, achieving a KGE value of 0.70.

352 It is noteworthy that EXP5 outperforms EXP1 except at the upstream position
 353 of the Yarlung Zangbo River at Lazi, even though their precipitation amounts are quite
 354 similar. This superior performance of EXP5 is primarily attributed to the improved cor-
 355 relation coefficient between the simulated and observed streamflow time series. We have

examined the relationship between the spatial correlation coefficient of streamflow and the catchment-wide spatial correlation coefficient of precipitation, as depicted in Figure 8. With the exception of the Lazi catchment, a relatively high correspondence in the temporal variations of streamflow is well-aligned with a relatively high correspondence in the spatial distribution of precipitation. This alignment is a consequence of water flow from various locations within the catchment converging at the catchment outlet, which influences the overall streamflow dynamics.

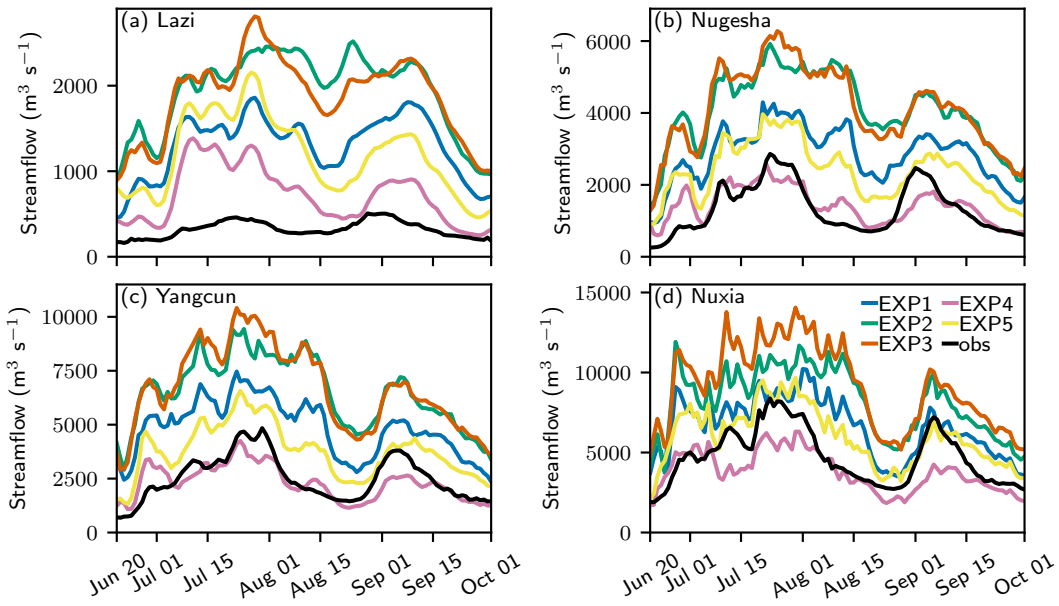


Figure 7. Comparison between streamflow observations and the streamflow estimated from the WRF experiments.

4 Conclusions

We have proposed a river network routing-based method for evaluating atmospheric models using streamflow observations. This method stands out from the hydrological model-based approach by relying on a substantially smaller set of assumptions regarding model structures and parameters. The streamlined nature of this approach bolsters its robustness and, in comparison to hydrological model-based evaluations, offers a more attractive alternative. This is especially true in mountainous basins, where the intricacies of runoff-generation processes frequently surpass the modeling capabilities of hydrological models.

Table 4. Kling–Gupta efficiency of the optimal streamflow estimate.

	Metric	LZ	NGS	YC	NX
EXP1	KGE	-3.12	-0.16	0.01	0.54
	α	3.76	1.14	1.26	1.06
	β	4.05	2.14	1.93	1.40
	r	0.81	0.80	0.79	0.79
EXP2	KGE	-5.34	-1.16	-0.72	0.19
	α	4.88	1.51	1.57	1.23
	β	6.00	3.08	2.60	1.74
	r	0.73	0.69	0.74	0.76
EXP3	KGE	-5.24	-1.21	-0.88	-0.09
	α	4.95	1.65	1.84	1.51
	β	5.82	3.11	2.67	1.95
	r	0.78	0.78	0.80	0.82
EXP4	KGE	-1.78	0.65	0.69	0.60
	α	3.46	0.72	0.77	0.72
	β	2.25	1.07	0.93	0.81
	r	0.65	0.80	0.81	0.79
EXP5	KGE	-3.59	0.19	0.45	0.70
	α	4.71	1.13	1.17	1.04
	β	3.68	1.79	1.51	1.27
	r	0.69	0.84	0.87	0.86

We applied this method to evaluate five numerical experiments, each featuring different configurations of WRF, in the simulated streamflow of the Yarlung Zangbo River, the largest river on the Tibetan Plateau. The streamflow evaluation complements the precipitation evaluation utilizing the GPM precipitation product. Our results indicate

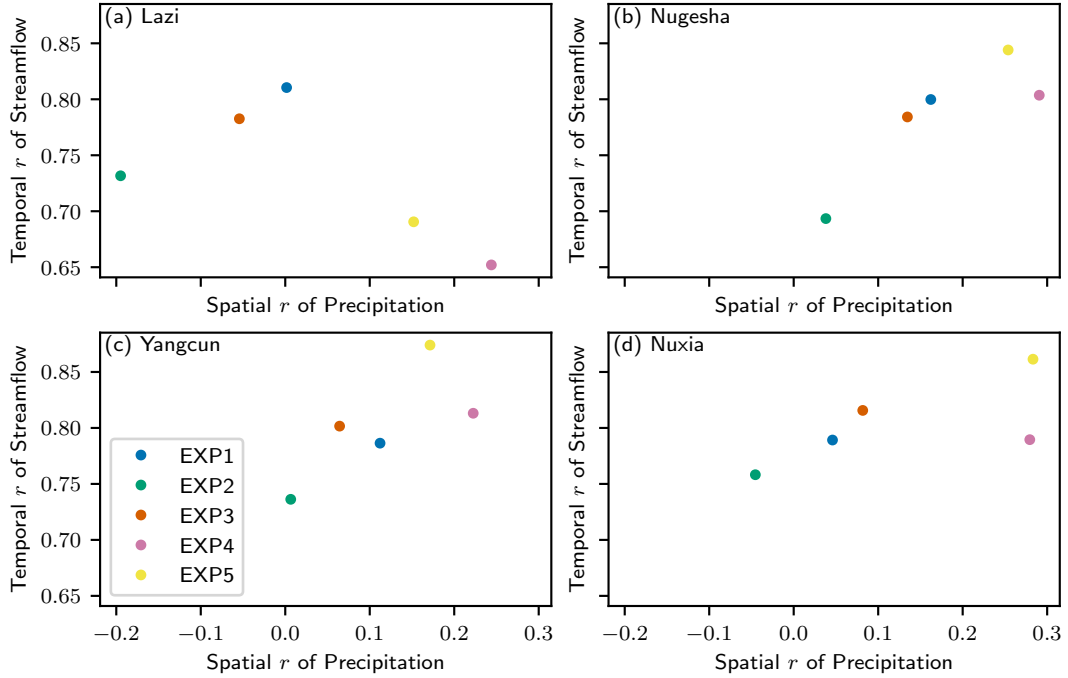


Figure 8. Relationship between the spatial correlation coefficient of precipitation and temporal correlation coefficient of streamflow. (a) The streamflow observed at Lazi and the precipitation averaged in the catchment of Lazi, (b) for Nugesha, (c) for Yangcun, and (d) for Nuxia.

a consistency between the proposed method's outcomes and those derived from the precipitation evaluation. Notably, the WRF configuration that integrated the Thompson cloud microphysics scheme, the RRTMG radiation scheme, and the YSU planetary boundary layer scheme exhibited optimal performance in simulating precipitation. This configuration's enhanced capability to replicate both the total amount and temporal patterns of precipitation is crucial for accurately estimating the mean and variability of streamflow.

Our proposed method enriches the evaluation of precipitation. While the shortwave radiation transfer process was found to have a minimal impact on the total amount of precipitation during the initial evaluation, it exerts a significant influence on streamflow simulation, particularly in the middle reaches between Lazi and Yangcun. Notably, the experiment that employed the Dudhia radiation scheme excelled in terms of the correlation coefficient and the Kling-Gupta Efficiency (KGE) at the downstream Nuxia gauge. This superior performance in modeling streamflow time series is attributed to the Dudhia scheme's effectiveness in capturing the spatial distribution of precipitation, under-

391 scoring the importance of accurate radiation transfer modeling in streamflow simulation.
 392 These findings reinforce the significance of the precipitation gradient in mountainous hy-
 393 drology, as discussed in (Immerzeel et al., 2014), and demonstrate the potential of our
 394 proposed method in evaluating atmospheric models in mountainous basins.

395 Open Research Section

396 The GPM IMERG final run precipitation product version 6 was used to evaluate
 397 the WRF-simulated precipitation (Huffman et al., 2019). The ERA5 reanalysis data (Hersbach
 398 et al., 2020) were used to drive the the WRF model version 4.3.1 (Powers et al., 2017)
 399 to simulate precipitation and runoff. The MERIT-Hydro flow direction and cumulative
 400 upstream area data (Yamazaki et al., 2019) were used to delineate the river network. The
 401 delineated river network and WRF-simulated precipitation and runoff is published at <https://doi.org/10.57760/sciencedb.11618> (Zheng, 2024). The streamflow observations for
 402 the Yarlung Zangbo River were obtained from China Three Gorges Corporation; how-
 403 ever, they are not shareable due to licensing restrictions.
 404

405 Acknowledgments

406 This study is supported by China Three Gorges Corporation (contract Z532302035)
 407 and the Natural Science Foundation of China (grants 42075165 and 42275178).

408 References

- 409 Behrangi, A., Andreadis, K., Fisher, J. B., Turk, F. J., Granger, S., Painter, T.,
 410 & Das, N. (2014). Satellite-based precipitation estimation and its ap-
 411 plication for streamflow prediction over mountainous western U.S. basins.
 412 *Journal of Applied Meteorology and Climatology*, 53(12), 2823–2842. doi:
 413 10.1175/JAMC-D-14-0056.1
- 414 Chen, S.-H., & Sun, W.-Y. (2002). A one-dimensional time dependent cloud model.
 415 *Journal of the Meteorological Society of Japan. Ser. II*, 80(1), 99–118. doi: 10
 416 .2151/jmsj.80.99
- 417 Clark, M. P., Kavetski, D., & Fenicia, F. (2011). Pursuing the method of multi-
 418 ple working hypotheses for hydrological modeling. *Water Resources Research*,
 419 47(9), 1–16. doi: 10.1029/2010WR009827
- 420 Cosgrove, B., Gochis, D., Flowers, T., Dugger, A., Ogden, F., Graziano, T., ...

- 421 Zhang, Y. (2024). NOAA's National Water Model: Advancing operational
422 hydrology through continental-scale modeling. *Journal of the American Water
423 Resources Association*, 60(2), 247–272. doi: 10.1111/1752-1688.13184
- 424 Cui, T., Li, Y., Yang, L., Nan, Y., Li, K., Tudaji, M., ... Tian, F. (2023).
425 Non-monotonic changes in Asian Water Towers' streamflow at increas-
426 ing warming levels. *Nature Communications*, 14(1), 1176. doi: 10.1038/
427 s41467-023-36804-6
- 428 Cunge, J. A. (1969). On the subject of a flood propagation computation method
429 (Muskingum method). *Journal of Hydraulic Research*, 7(2), 205–230. doi: 10
430 .1080/00221686909500264
- 431 David, C. H., Maidment, D. R., Niu, G.-Y., Yang, Z.-L., Habets, F., & Eijkhout, V.
432 (2011). River network routing on the NHDPlus dataset. *Journal of Hydrome-
433 teorology*, 12(5), 913–934. doi: 10.1175/2011JHM1345.1
- 434 Denis, B., Laprise, R., Caya, D., & Côté, J. (2002). Downscaling ability of one-way
435 nested regional climate models: the Big-Brother Experiment. *Climate Dynam-
436 ics*, 18(8), 627–646. doi: 10.1007/s00382-001-0201-0
- 437 Dudhia, J. (1989). Numerical study of convection observed during the winter
438 monsoon experiment using a mesoscale two-dimensional model. *Journal of
439 the Atmospheric Sciences*, 46(20), 3077–3107. doi: 10.1175/1520-0469(1989)
440 046<3077:NSOCOD>2.0.CO;2
- 441 Fenton, J. D. (2019). Flood routing methods. *Journal of Hydrology*, 570, 251–264.
442 doi: 10.1016/j.jhydrol.2019.01.006
- 443 Getirana, A. C., & Paiva, R. C. (2013). Mapping large-scale river flow hydraulics
444 in the Amazon Basin. *Water Resources Research*, 49(5), 2437–2445. doi: 10
445 .1002/wrcr.20212
- 446 Gupta, H. V., Kling, H., Yilmaz, K. K., & Martinez, G. F. (2009). Decomposition
447 of the mean squared error and NSE performance criteria: Implications for im-
448 proving hydrological modelling. *Journal of Hydrology*, 377(1-2), 80–91. doi:
449 10.1016/j.jhydrol.2009.08.003
- 450 Henn, B., Clark, M. P., Kavetski, D., & Lundquist, J. D. (2015). Estimating moun-
451 tain basin-mean precipitation from streamflow using Bayesian inference. *Water
452 Resources Research*, 51(10), 8012–8033. doi: 10.1002/2014WR016736
- 453 Henn, B., Clark, M. P., Kavetski, D., McGurk, B., Painter, T. H., & Lundquist,

- 454 J. D. (2016). Combining snow, streamflow, and precipitation gauge observa-
455 tions to infer basin-mean precipitation. *Water Resources Research*, 52(11),
456 8700–8723. doi: 10.1002/2015WR018564
- 457 Hersbach, H., Bell, B., Berrisford, P., Hirahara, S., Horányi, A., Muñoz-Sabater, J.,
458 ... Thépaut, J.-N. (2020). The ERA5 global reanalysis. *Quarterly Journal of*
459 *the Royal Meteorological Society*, 146(730), 1999–2049. doi: 10.1002/qj.3803
- 460 Hong, S.-Y., & Lim, J.-O. J. (2006). The WRF Single-Moment 6-Class Microphysics
461 Scheme (WSM6). *Asia-Pacific Journal of Atmospheric Sciences*, 42(2), 129–
462 151.
- 463 Hong, S.-Y., Noh, Y., & Dudhia, J. (2006). A new vertical diffusion package with an
464 explicit treatment of entrainment processes. *Monthly Weather Review*, 134(9),
465 2318–2341. doi: 10.1175/MWR3199.1
- 466 Huffman, G. J., Stocker, E. F., Bolvin, D. T., Nelkin, E. J., & Tan, J. (2019).
467 *GPM IMERG final precipitation L3 half hourly 0.1 degree x 0.1 degree V06*
468 (*GPM_3IMERGHH*). NASA/GSFC/SED/ESD/GCDC/GESDISC. Retrieved
469 2022-12-05, from <https://doi.org/10.5067/GPM/IMERG/3B-HH/06> doi:
470 10.5067/GPM/IMERG/3B-HH/06
- 471 Iacono, M. J., Delamere, J. S., Mlawer, E. J., Shephard, M. W., Clough, S. A., &
472 Collins, W. D. (2008). Radiative forcing by long-lived greenhouse gases: Cal-
473 culations with the AER radiative transfer models. *Journal of Geophysical*
474 *Research: Atmospheres*, 113(D13), D13103. doi: 10.1029/2008JD009944
- 475 Immerzeel, W. W., Petersen, L., Ragettli, S., & Pellicciotti, F. (2014). The impor-
476 tance of observed gradients of air temperature and precipitation for modeling
477 runoff from a glacierized watershed in the Nepalese Himalayas. *Water Re-*
478 *sources Research*, 50(3), 2212–2226. doi: 10.1002/2013WR014506
- 479 Janjić, Z. I. (1994). The step-mountain Eta coordinate model: further developments
480 of the convection, viscous sublayer, and turbulence closure schemes. *Monthly*
481 *Weather Review*, 122(5), 927–945. doi: 10.1175/1520-0493(1994)122<0927:
482 TSMECM>2.0.CO;2
- 483 Jiang, Y., Yang, K., Li, X., Zhang, W., Shen, Y., Chen, Y., & Li, X. (2022).
484 Atmospheric simulation-based precipitation datasets outperform satellite-
485 based products in closing basin-wide water budget in the eastern Tibetan
486 Plateau. *International Journal of Climatology*, 42(14), 7252–7268. doi:

- 487 10.1002/joc.7642
- 488 Jiang, Y., Yang, K., Yang, H., Lu, H., Chen, Y., Zhou, X., ... Wang, Y. (2022).
 489 Characterizing basin-scale precipitation gradients in the Third Pole region
 490 using a high-resolution atmospheric simulation-based dataset. *Hydrology and*
 491 *Earth System Sciences*, 26(17), 4587–4601. doi: 10.5194/hess-26-4587-2022
- 492 Kirchner, J. W. (2009). Catchments as simple dynamical systems: Catchment char-
 493 acterization, rainfall-runoff modeling, and doing hydrology backward. *Water*
 494 *Resources Research*, 45(2), W02429. doi: 10.1029/2008WR006912
- 495 Koussis, A. D. (1978). Theoretical estimation of flood routing parameters. *Journal*
 496 *of the Hydraulics Division*, 104(1), 109–115. doi: 10.1061/JYCEAJ.0004909
- 497 Kraaijenbrink, P. D. A., Stigter, E. E., Yao, T., & Immerzeel, W. W. (2021).
 498 Climate change decisive for Asia's snow meltwater supply. *Nature Climate*
 499 *Change*, 11(7), 591–597. doi: 10.1038/s41558-021-01074-x
- 500 Krier, R., Matgen, P., Goergen, K., Pfister, L., Hoffmann, L., Kirchner, J. W., ...
 501 Savenije, H. H. G. (2012). Inferring catchment precipitation by doing hydro-
 502 logy backward: A test in 24 small and mesoscale catchments in Luxembourg.
 503 *Water Resources Research*, 48(10), W10525. doi: 10.1029/2011WR010657
- 504 Lei, X., Lin, P., Zheng, H., Fei, W., Yin, Z., & Ren, H. (2024). Beyond model
 505 parameters: on the meteorological forcing and process parameterization un-
 506 certainties in runoff simulation for a poorly-gauged high-altitude river basin.
 507 *Journal of Hydrology (under review)*.
- 508 Li, G., Chen, H., Xu, M., Zhao, C., Zhong, L., Li, R., ... Gao, Y. (2022). Impacts of
 509 topographic complexity on modeling moisture transport and precipitation over
 510 the Tibetan Plateau in summer. *Advances in Atmospheric Sciences*, 39(7),
 511 1151–1166. doi: 10.1007/s00376-022-1409-7
- 512 Liang, J., Yang, Z.-L., & Lin, P. (2019). Systematic hydrological evaluation of the
 513 Noah-MP land surface model over China. *Advances in Atmospheric Sciences*,
 514 36(11), 1171–1187. doi: 10.1007/s00376-019-9016-y
- 515 Lin, C., Chen, D., Yang, K., & Ou, T. (2018). Impact of model resolution on sim-
 516 ulating the water vapor transport through the central Himalayas: implication
 517 for models' wet bias over the Tibetan Plateau. *Climate Dynamics*, 51(9),
 518 3195–3207. doi: 10.1007/s00382-018-4074-x
- 519 Lin, P., Hopper, L. J., Yang, Z.-L., Lenz, M., & Zeitler, J. W. (2018). Insights into

- 520 hydrometeorological factors constraining flood prediction skill during the May
521 and October 2015 Texas Hill Country flood events. *Journal of Hydrometeorol-*
522 *ogy*, 19(8), 1339–1361. doi: 10.1175/JHM-D-18-0038.1
- 523 Lin, P., Pan, M., Beck, H. E., Yang, Y., Yamazaki, D., Frasson, R., ... Wood, E. F.
524 (2019). Global reconstruction of naturalized river flows at 2.94 million reaches.
525 *Water Resources Research*, 55(8), 6499–6516. doi: 10.1029/2019WR025287
- 526 Lin, P., Pan, M., Wood, E. F., Yamazaki, D., & Allen, G. H. (2021). A new vector-
527 based global river network dataset accounting for variable drainage density.
528 *Scientific Data*, 8(1), 28. doi: 10.1038/s41597-021-00819-9
- 529 Lin, P., Yang, Z.-L., Gochis, D. J., Yu, W., Maidment, D. R., Somos-Valenzuela,
530 M. A., & David, C. H. (2018). Implementation of a vector-based river network
531 routing scheme in the community WRF-Hydro modeling framework for flood
532 discharge simulation. *Environmental Modelling & Software*, 107, 1–11. doi:
533 10.1016/j.envsoft.2018.05.018
- 534 Lundquist, J., Hughes, M., Gutmann, E., & Kapnick, S. (2019). Our skill in mod-
535 eling mountain rain and snow is bypassing the skill of our observational net-
536 works. *Bulletin of the American Meteorological Society*, 100(12), 2473–2490.
537 doi: 10.1175/bams-d-19-0001.1
- 538 Lv, M., Xu, Z., & Yang, Z. (2020). Cloud resolving WRF simulations of precipi-
539 tation and soil moisture over the central Tibetan Plateau: an assessment of
540 various physics options. *Earth and Space Science*, 7(2), e2019EA000865. doi:
541 10.1029/2019EA000865
- 542 Ma, M., Ou, T., Liu, D., Wang, S., Fang, J., & Tang, J. (2023). Summer re-
543 gional climate simulations over Tibetan Plateau: from gray zone to con-
544 vection permitting scale. *Climate Dynamics*, 60(1), 301–322. doi:
545 10.1007/s00382-022-06314-0
- 546 Miao, C., Immerzeel, W. W., Xu, B., Yang, K., Duan, Q., & Li, X. (2024). Un-
547 derstanding the Asian water tower requires a redesigned precipitation obser-
548 vation strategy. *Proceedings of the National Academy of Sciences*, 121(23),
549 e2403557121. doi: 10.1073/pnas.2403557121
- 550 Mlawer, E. J., Taubman, S. J., Brown, P. D., Iacono, M. J., & Clough, S. A. (1997).
551 Radiative transfer for inhomogeneous atmospheres: RRTM, a validated
552 correlated-k model for the longwave. *Journal of Geophysical Research: At-*

- mospheres, 102(D14), 16663–16682. doi: 10.1029/97JD00237

Mooney, P. A., Broderick, C., Bruyère, C. L., Mulligan, F. J., & Prein, A. F. (2017). Clustering of observed diurnal cycles of precipitation over the United States for evaluation of a WRF multiphysics regional climate ensemble. *Journal of Climate*, 30(22), 9267–9286. doi: 10.1175/JCLI-D-16-0851.1

Moussa, R., & Bocquillon, C. (1996). Criteria for the choice of flood-routing methods in natural channels. *Journal of Hydrology*, 186(1-4), 1–30. doi: 10.1016/S0022-1694(96)03045-4

Niu, G.-Y., Yang, Z.-L., Mitchell, K. E., Chen, F., Ek, M. B., Barlage, M., ... Xia, Y. (2011). The community Noah land surface model with multiparameterization options (Noah-MP): 1. Model description and evaluation with local-scale measurements. *Journal of Geophysical Research: Atmospheres*, 116(D12), D12109. doi: 10.1029/2010JD015139

Pang, J., Zhang, H., Xu, Q., Wang, Y., Wang, Y., Zhang, O., & Hao, J. (2020). Hydrological evaluation of open-access precipitation data using SWAT at multiple temporal and spatial scales. *Hydrology and Earth System Sciences*, 24(7), 3603–3626. doi: 10.5194/hess-24-3603-2020

Ponce, V. M., Simons, D. B., & Li, R.-M. (1978). Applicability of kinematic and diffusion models. *Journal of the Hydraulics Division*, 104(3), 353–360. doi: 10.1061/JYCEAJ.0004958

Powers, J. G., Klemp, J. B., Skamarock, W. C., Davis, C. A., Dudhia, J., Gill, D. O., ... Duda, M. G. (2017). The Weather Research and Forecasting model: overview, system efforts, and future directions. *Bulletin of the American Meteorological Society*, 98(8), 1717–1737. doi: 10.1175/bams-d-15-00308.1

Prein, A. F., Ban, N., Ou, T., Tang, J., Sakaguchi, K., Collier, E., ... Chen, D. (2023). Towards ensemble-based kilometer-scale climate simulations over the Third Pole region. *Climate Dynamics*, 60(11), 4055–4081. doi: 10.1007/s00382-022-06543-3

Prein, A. F., Langhans, W., Fosser, G., Ferrone, A., Ban, N., Goergen, K., ... Leung, R. (2015). A review on regional convection-permitting climate modeling: Demonstrations, prospects, and challenges. *Reviews of Geophysics*, 53(2), 323–361. doi: 10.1002/2014RG000475

Renard, B., Kavetski, D., Kuczera, G., Thyer, M., & Franks, S. W. (2010). Un-

- 586 derstanding predictive uncertainty in hydrologic modeling: The challenge of
587 identifying input and structural errors. *Water Resources Research*, 46(5),
588 W05521. doi: 10.1029/2009WR008328
- 589 Senatore, A., Mendicino, G., Gochis, D. J., Yu, W., Yates, D. N., & Kunstmann,
590 H. (2015). Fully coupled atmosphere-hydrology simulations for the central
591 Mediterranean: Impact of enhanced hydrological parameterization for short
592 and long time scales. *Journal of Advances in Modeling Earth Systems*, 7(4),
593 1693–1715. doi: 10.1002/2015MS000510
- 594 Sugimoto, S., Ueno, K., Fujinami, H., Nasuno, T., Sato, T., & Takahashi, H. G.
595 (2021). Cloud-resolving-model simulations of nocturnal precipitation over
596 the Himalayan slopes and foothills. *Journal of Hydrometeorology*, 22(12),
597 3171–3188. doi: 10.1175/JHM-D-21-0103.1
- 598 Thompson, G., Field, P. R., Rasmussen, R. M., & Hall, W. D. (2008). Explicit fore-
599 casts of winter precipitation using an improved bulk microphysics scheme. part
600 II: implementation of a new snow parameterization. *Monthly Weather Review*,
601 136(12), 5095–5115. doi: 10.1175/2008MWR2387.1
- 602 van Tiel, M., Aubry-Wake, C., Somers, L., Andermann, C., Avanzi, F., Baraer, M.,
603 ... Yapiyev, V. (2024). Cryosphere-groundwater connectivity is a miss-
604 ing link in the mountain water cycle. *Nature Water*, 2(7), 624–637. doi:
605 10.1038/s44221-024-00277-8
- 606 Wagner, S., Fersch, B., Yuan, F., Yu, Z., & Kunstmann, H. (2016). Fully coupled
607 atmospheric-hydrological modeling at regional and long-term scales: Devel-
608 opment, application, and analysis of WRF-HMS. *Water Resources Research*,
609 52(4), 3187–3211. doi: 10.1002/2015wr018185
- 610 Wang, S., Zheng, H., Lin, P., Zheng, X., & Yang, Z.-L. (2019). Evaluation and un-
611 certainty attribution of the simulated streamflow from NoahMP-RAPID over a
612 high-altitude mountainous basin. *Chinese Science Bulletin (in Chinese)*, 64(4),
613 444–455. doi: 10.1360/N972018-00598
- 614 Wang, T., Zhao, Y., Xu, C., Ciais, P., Liu, D., Yang, H., ... Yao, T. (2021).
615 Atmospheric dynamic constraints on Tibetan Plateau freshwater under
616 Paris climate targets. *Nature Climate Change*, 11(3), 219–225. doi:
617 10.1038/s41558-020-00974-8
- 618 Wang, X., Tolksdorf, V., Otto, M., & Scherer, D. (2021). WRF-based dynamical

- 619 downscaling of ERA5 reanalysis data for High Mountain Asia: Towards a new
620 version of the High Asia Refined analysis. *International Journal of Climatology*,
621 41(1), 743–762. doi: 10.1002/joc.6686
- 622 Wang, Y., Zeng, X., Xu, X., Welty, J., Lenschow, D. H., Zhou, M., & Zhao, Y.
623 (2020). Why are there more summer afternoon low clouds over the Tibetan
624 Plateau compared to Eastern China? *Geophysical Research Letters*, 47(23),
625 e2020GL089665. doi: 10.1029/2020gl089665
- 626 Yamazaki, D., Ikeshima, D., Sosa, J., Bates, P. D., Allen, G. H., & Pavelsky, T. M.
627 (2019). MERIT Hydro: A high-resolution global hydrography map based on
628 latest topography dataset. *Water Resources Research*, 55(6), 5053–5073. doi:
629 10.1029/2019wr024873
- 630 Yamazaki, D., Ikeshima, D., Tawatari, R., Yamaguchi, T., O’Loughlin, F., Neal,
631 J. C., … Bates, P. D. (2017). A high-accuracy map of global ter-
632 rain elevations. *Geophysical Research Letters*, 44(11), 5844–5853. doi:
633 10.1002/2017GL072874
- 634 Yang, X., Wei, C., Li, Z., Yang, H., & Zheng, H. (2024). A stream-order family and
635 order-based parallel river network routing method. *Water*, 16(14), 1965. doi:
636 10.3390/w16141965
- 637 Yang, Z.-L., Niu, G.-Y., Mitchell, K. E., Chen, F., Ek, M. B., Barlage, M., …
638 Xia, Y. (2011). The community Noah land surface model with multipa-
639 rameterization options (Noah-MP): 2. Evaluation over global river basins.
640 *Journal of Geophysical Research: Atmospheres*, 116(D12), D12110. doi:
641 10.1029/2010JD015140
- 642 Yao, T., Xue, Y., Chen, D., Chen, F., Thompson, L., Cui, P., … Li, Q. (2019).
643 Recent Third Pole’s rapid warming accompanies cryospheric melt and wa-
644 ter cycle intensification and interactions between monsoon and environ-
645 ment: multidisciplinary approach with observations, modeling, and analy-
646 sis. *Bulletin of the American Meteorological Society*, 100(3), 423–444. doi:
647 10.1175/bams-d-17-0057.1
- 648 Yuan, X., Yang, K., Lu, H., Wang, Y., & Ma, X. (2023). Impacts of moisture trans-
649 port through and over the Yarlung Tsangpo Grand Canyon on precipitation
650 in the eastern Tibetan Plateau. *Atmospheric Research*, 282, 106533. doi:
651 10.1016/j.atmosres.2022.106533

- 652 Zheng, H. (2024). *Evaluating atmospheric model parameterization schemes with*
653 *river network routing and streamflow observations: A case study of the Yarlung*
654 *Zangbo River on the Tibetan Plateau.* <https://www.scidb.cn>: Science Data
655 Bank. doi: 10.57760/sciedb.11618
- 656 Zheng, H., Fei, W., Yang, Z.-L., Wei, J., Zhao, L., Li, L., & Wang, S. (2023). An
657 ensemble of 48 physically perturbed model estimates of the 1/8° terrestrial
658 water budget over the conterminous United States, 1980–2015. *Earth System*
659 *Science Data*, 15(7), 2755–2780. doi: 10.5194/essd-15-2755-2023
- 660 Zheng, H., Yang, Z.-L., Lin, P., Wu, W.-Y., Li, L., Xu, Z., ... Wang, S. (2020).
661 Falsification-oriented signature-based evaluation for guiding the develop-
662 ment of land surface models and the enhancement of observations. *Jour-*
663 *nal of Advances in Modeling Earth Systems*, 12(12), e2020MS002132. doi:
664 10.1029/2020MS002132
- 665 Zhou, X., Yang, K., Ouyang, L., Wang, Y., Jiang, Y., Li, X., ... Prein, A. (2021).
666 Added value of kilometer-scale modeling over the third pole region: a
667 CORDEX-CPTP pilot study. *Climate Dynamics*, 57(7), 1673–1687. doi:
668 10.1007/s00382-021-05653-8